A hydrogen bond network in the active site of *Anabaena* ferredoxin-NADP+ reductase modulates its catalytic efficiency

Q1 Ana Sánchez-Azqueta [a,b], Beatriz Herguedas [a,b], Ramón Hurtado-Guerrero [a,b,c], Manuel Hervás [d], José A. Navarro [d], Marta Martínez-Júlvez [a,b], Milagros Medina [a,b,*]

[a] *Departamento de Bioquímica y Biología Molecular y Celular, Facultad de Ciencias, Universidad de Zaragoza, Zaragoza, Spain*
[b] *Institute of Biocomputation and Physics of Complex Systems (BIFI)-Joint Unit BIFI-IQFR (CSIC), Universidad de Zaragoza, Zaragoza, Spain*
[c] *Fundación ARAID, Gobierno de Aragón, Spain*
[d] *Instituto de Bioquímica Vegetal y Fotosíntesis, cicCartuja, Universidad de Sevilla & CSIC, Sevilla, Spain*

ARTICLE INFO

ABSTRACT

Ferredoxin-NADP+ reductase (FNR) catalyses the production of NADPH in photosynthetic organisms, where its FAD cofactor takes two electrons from two reduced ferredoxin (Fd) molecules in two sequential steps, and transfers them to NADP+ in a single hydride transfer (HT) step. Despite the good knowledge of this catalytic machinery, additional roles can still be envisaged for already reported key residues, and new features are added to residues not previously identified as having a particular role in the mechanism. Here, we analyse for the first time the role of Ser59 in *Anabaena* FNR, a residue suggested by recent theoretical simulations as putatively involved in competent binding of the coenzyme in the active site by cooperating with Ser80. We show that Ser59 indirectly modulates the geometry of the active site, the interaction with substrates and the electronic properties of the isoalloxazine ring, and in consequence the electron transfer (ET) and HT processes. Additionally, we revise the role of Tyr79 and Ser80, previously investigated in homologous enzymes from plants. Our results probe that the active site of FNR is tuned by a H-bond network that involves the side-chains of these residues and that results to critical optimal substrate binding, exchange of electrons and, particularly, competent disposition of the C4n (hydride acceptor/donor) of the nicotinamide moiety of the coenzyme during the reversible HT event.
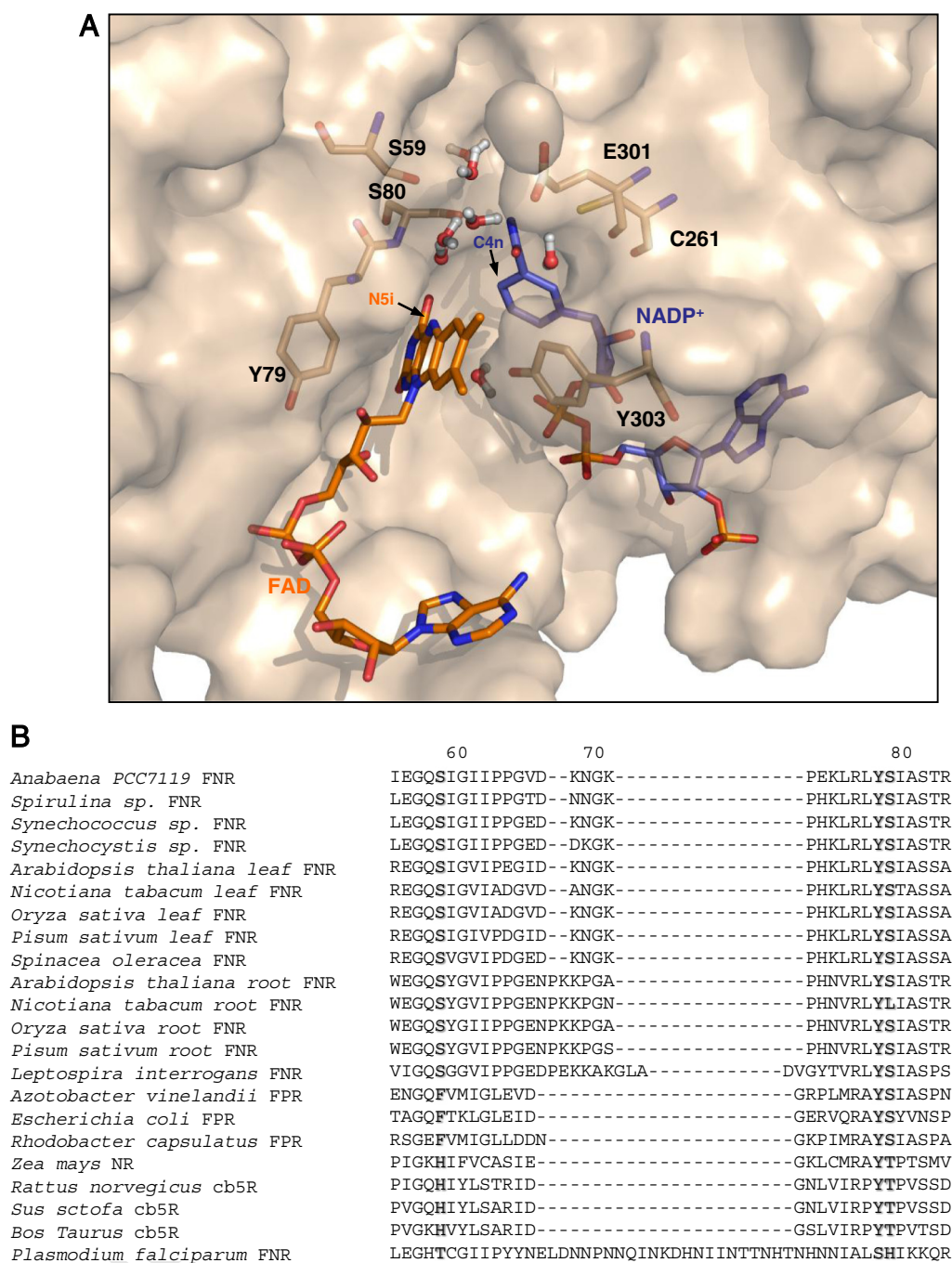
© 2013 Elsevier B.V. All rights reserved.

1. Introduction

In the photosynthetic electron transfer (ET) chain of plants, algae and cyanobacteria, the isoalloxazine ring of the FAD cofactor of ferredoxin-NADP+ reductase (FNR) gets reduced to its hydroquinone state by sequentially accepting two electrons from two ferredoxin (Fd) molecules. Subsequently, it transfers a hydride from the N5 atom (N5Hi) of the isoalloxazine of its FAD cofactor to the nicotinamide C4 atom of NADP+ (C4n) to provide the cell with reduction power in the form of NADPH [1–3]. The overall ET process from Fd to NADP+ is reversible, with transitory ternary complexes, Fd:FNR:NADP+, formed during catalysis [4]. Structural, mutational and theoretical studies revealed residues on the protein surface and in the isoalloxazine environment involved in the interaction and ET with the protein partner, contributing to the optimal architecture of the active site for proton and electron transfer, as well as playing key roles in the catalytic binding of the nicotinamide moiety of the coenzyme (NMN) during the hydride transfer (HT) event [5–13]. Among them, a particular role is proposed for the C-terminal Tyr (Tyr303 in *Anabaena* FNR (*An*FNR), numbering used herein) (Fig. 1A). This residue stacks at the *re*-face of the isoalloxazine ring of FAD, modulates its midpoint reduction potential and reduces the probability of a too strong stacking interaction between the

Fig. 1. Key residues at the *An*FNR active site. (A) Surface representation of the active site environment at the equilibrium of a MD simulation of a theoretical catalytically competent WT FNR$_{hq}$:NADP$^+$ complex [15]. NADP$^+$, FAD, and selected key side-chains are shown in sticks with C in blue, orange and wheat, respectively. Selected water molecules at the active site are also shown as balls and sticks. (B) Sequence alignment of different members of the FNR superfamily (ClustalW2). Position of residues equivalent to those mutated in this work is shown in bold.

isoalloxazine and nicotinamide rings, thus contributing to the optimal geometry among the N5i, the C4n and the hydrogen that have to be transferred between them [5,12,14–18]. A second highly conserved aromatic side-chain, Tyr79, stacks at the isoalloxazine *si*-face with its hydroxyl H-bonding the 4′-ribityl hydroxyl of FAD, which is also connected through a complex H-bond network assisted by water molecules to the C2 of the isoalloxazine and to the side-chain Arg100 [8,19–22]. Other key highly conserved residues at the active site are the neighbours of Tyr303 at the *re*-face: Ser80, Cys261 and Glu301 [3,8,11,15,23–26]. They contribute to the fine modulation of the FAD midpoint reduction potential, the affinity for Fd, the architecture of the catalytically competent complex, and/or the ET and HT rates [5,7,10,11,26–28]. Despite the fact that structural changes detected upon spinach FNR reduction are minor, they implicate a slight approach of the hydroxyl of Ser96 (Ser80 in *An*FNR) to N5i that loses its H-bond with Glu312 (Glu301 in *An*FNR) leading to the displacement of Tyr314 (Tyr303 in *An*FNR) away from the flavin ring (decreasing the π–π stacking with the reduced isoalloxazine), as well as the displacement of two highly conserved water molecules, W406 and W571, (W404 and W457 in *An*FNR) located near the

ribityl of FAD [29]. Theoretical calculations for the HT process between the isoalloxazine and the nicotinamide of the coenzyme, also supported by experimental evidences, confirm that the sulfhydryl group of Cys261 contributes to the approach of the N7n in the NMN amide to the isoalloxazine along the reaction path, while the O7n in the same amide H-bonds Ser80 (Fig. 1A) [18,28]. Ser80 is kept in the C4n and N5Hi atom environments along the reaction coordinate, contributing to a network of interactions involving the isoalloxazine ring, the nicotinamide ring, Cys261 and Ser80 itself (Fig. 1A). This network facilitates the approach of the reacting N5Hi and C4n atoms, and therefore, it is expected to contribute towards the adequate geometry for the chemical step of the reaction [6,10,11,15]. Thus, the architecture of the active site for the HT event must precisely contribute to the orientation of the N5Hi of the FAD_{hq} isoalloxazine and the C4n of the coenzyme nicotinamide rings and, therefore, to the efficiency of the HT process [14–16]. Molecular dynamics (MD) simulations additionally indicated that H-bonds between the side-chains of Ser80 and Ser59 are highly populated (Fig. 1A) [15]. These side-chains also H-bond Glu301, proposed by theoretical and experimental evidences to switch positions in and out of the active site to provide a pathway for proton transfer between the external medium and N5i, via Ser80, during FNR reduction by Fd [14,27]. This route might also include Ser59, highly conserved in the plant type FNR family (Fig. 1B) [21,29].

In this study, we further analyse the roles of Ser59, Tyr79 and Ser80 in AnFNR during catalysis to better understand the function of the interacting network to which they contribute to within the active site. The presented results provide information about the role of this interacting network, indicating that it modulates the electronic environment of the isoalloxazine ring and influences the ET process from Fd, as well as the active site geometry during HT. Particularly, we show for the first time that Ser59 indirectly modulates the geometry of the active site, the interaction with substrates and the efficiency of the ET and HT processes. Additionally, the roles of these side-chains in the competent placement of the C4n (hydride acceptor/donor atom) and in the tunnelling contribution during the HT event have been analysed, being particularly relevant those of Ser80.

2. Materials and methods

2.1. Biological material

pET28a-AnFNR plasmids containing the S59A, S80A or Y79F mutations were obtained from the company Mutagenex® and used to produce and purify the corresponding proteins from *Escherichia coli* cultures as previously reported [30]. Samples were prepared in 50 mM Tris/HCl, pH 8.0. S80A FNR was further purified using a HiPrep™ 26/60 Sephacryl™ S-200 HR column (*GE Healthcare*). FNR_{hq} variants were obtained by anaerobic photoreduction of the samples in the presence of 2 μM 5-deazariboflavin (dRf) and 3 mM EDTA in 50 mM Tris/HCl, pH 8.0, by irradiation from a 250 W light source [31]. Deuterated FNR_{hq} (D-FNR_{hq}) variants were produced by photoreduction with EDTA and dRf of the corresponding FNR_{ox} previously dialysed in 50 mM Tris/DCl, pD ~ 8.0 in D_2O. NADPD (4R-form, with the deuterium in the A face of the nicotinamide) was produced and purified as described [14,32]. *Anabaena* Fd (AnFd) was produced as previously described [12].

2.2. Spectroscopic assays

UV/vis spectra were recorded in a Cary-100 spectrophotometer. The molar absorption coefficient for each FNR variant was spectrophotometrically determined by thermal denaturation of the protein for 10 min at 90 °C, followed by centrifugation and separation of the precipitated apoprotein, and spectroscopic quantification of the FAD released to the supernatant [33]. Interaction parameters with $NADP^+$, NAD^+ and Fd were determined by difference absorption spectroscopy at 25 °C in 50 mM Tris/HCl, pH 8.0, as previously described [7,34]. Titrations were carried out by adding aliquots of 1 mM $NADP^+$ or Fd, and 50 mM NAD^+ to 20–80 μM FNR solutions. Errors in the determination of K_d and $\Delta\varepsilon$ were ± 10% and ± 5%, respectively.

2.3. Determination of midpoint reduction potentials of the FNR variants

Midpoint reduction potentials for the ox/hq couple ($E_{ox/hq}$, two-electron reduction process) of WT, S59A, Y79F, and S80A FNRs were determined at 25 °C by potentiometric titration under anaerobic conditions using a gold electrode and a calomel electrode as reference ($E_m = +244.4$ mV at 25 °C). Due to the low degree of FNR semiquinone stabilisation it was not possible to measure the potential for the two one-electron steps. Typically, the solution contained ~20 μM FNR, 50 mM Tris/HCl buffer, pH 8.0, 3 mM EDTA and 2 μM dRf. 0.02% n-dodecyl-β-D-maltoside was also added to S80A FNR to increase its stability. Methylviologen ($E_m = -446$ mV) and benzylviologen ($E_m = -359$ mV) were additionally used as mediators. Solutions were made anaerobic over a 2–4 h period. Stepwise reduction of the protein was achieved by photoreduction using the equipment previously described [35]. The system was considered equilibrated when the potential (E), measured with a Fluke 177 true-RMS multimeter, remained stable for at least 10 min. The UV/vis absorbance spectrum was then recorded and used to determine [FNR_{ox}] and [FNR_{hq}] at the equilibrium after each reduction step. $E_{ox/hq}$ was calculated by linear regression analysis according to the Nernst equation. The values of each one-electron single step, $E_{ox/sq}$ and $E_{sq/hq}$, were derived from Eqs. (1) and (2) using the experimentally determined $E_{ox/hq}$ and the molar faction of the maximum percentage of SQ stabilised.

$$E_{ox/sq} - E_{sq/hq} = 0.11 * \log\frac{2[SQ]}{1-[SQ]};\qquad(1)$$

$$\frac{E_{ox/sq} + E_{sq/hq}}{2} = E_{ox/hq}.\qquad(2)$$

Error in the determined $E_{ox/hq}$, $E_{ox/sq}$ and $E_{sq/hq}$ values was estimated to be ± 5 mV.

2.4. Steady-state kinetics measurements

The diaphorase activity of FNR was determined in a double beam Cary-100 spectrophotometer using either 2,6-dichlorophenolindophenol (DCPIP) ($\Delta\varepsilon_{620\ nm}$ 21 mM^{-1} cm^{-1}) or $K_3Fe(CN)_6$ ($\Delta\varepsilon_{420\ nm}$ 1.05 mM^{-1} cm^{-1}) as two- or one-electron acceptors, respectively. The final reaction mixture contained 4 nM FNR, 0.1 mM DCPIP or 1.5 mM $K_3Fe(CN)_6$, and NADPH in the range 0–200 μM, while the reference cuvette contained 0.06 mM DCPIP when using this acceptor. Higher concentrations of FNR (1 μM) and/or nucleotide (0–5 mM) were required for the analysis of the reactions with NADH. The NADPH-dependent cytochrome c reductase activity was determined using AnFd, and horse heart cytochrome c (Cytc) as final electron acceptor. Reaction mixtures contained 4 nM FNR, 200 μM NADPH, 0.75 mg/ml Cytc and 0–15 μM AnFd. All measurements were carried out in 50 mM Tris/HCl, pH 8.0, at 25 °C. K_m and k_{cat} values were obtained by fitting the dependence of the observed initial rates on coenzyme concentration to the Michaelis–Menten equation. Estimated errors in K_m and k_{cat} were ± 20% and ± 10%, respectively.

2.5. Laser-flash induced kinetics

Laser-flash experiments were performed anaerobically at 25 °C in a 1 cm path-length cuvette using EDTA as electron donor and dRf as photosensitizer as previously described [7,36]. The standard reaction mixture contained, in a final volume of 1.5 mL, 4 mM sodium phosphate,

pH 7.0, 2 mM EDTA and 100 μM dRf (low ionic strength (I) buffer). The laser-generated dRf triplet abstracts a hydrogen atom from EDTA which is present in large excess and produces the dRf semiquinone (dRfH•) which, in competition with its own disproportionation, reduces the oxidised protein. Direct reduction of AnFNR$_{ox}$ by the laser-flash photoreduced dRf (dRfH•) was followed by measuring the decrease of absorbance in the flavin band-I maxima at 458 nm. When both Fd and FNR are present simultaneously in the solution, the flash generated dRfH• reacts almost exclusively with free Fd$_{ox}$, and thus the subsequent ET process from the generated Fd$_{rd}$ to FNR$_{ox}$ can be monitored [7,12,13]. FNR reduction by Fd$_{rd}$ was followed as the increase of absorbance at 600 nm, a wavelength at which the production of FNR$_{sq}$ can be monitored as FNR$_{ox}$ is reduced by Fd$_{rd}$. Control experiments collected at 489–500 nm, an isosbestic point of the FNR$_{ox/sq}$ couple, allowed to monitor the oxidation of Fd$_{rd}$, yielding rate constants that were the same, within experimental error, as those determined from the 600 nm data, as expected from the two step mechanism shown in Eq. (3). For these experiments, 40 μM AnFd and AnFNR at varying concentrations were added to the standard reaction mixture, either in the absence or in the presence of 100 mM NaCl. For I dependence experiments, small amounts of a concentrated solution of 5 M NaCl were added to a reaction cuvette containing the low I buffer, 40 μM AnFd and 30 μM AnFNR. All experiments were performed under pseudo-first-order conditions, for which the amount of acceptor (FNR$_{ox}$) was maintained well in excess over the amount of the generated Fd$_{rd}$ (<1 μM). Each kinetic trace was the average of 8–15 measurements. All kinetic traces were fitted to monoexponential curves by using the Marquardt method to obtain the observed rate constants (k_{obs}). Linear fittings of k_{obs} values on FNR concentration allowed obtaining second-order bimolecular rate constants (k_2). Non-linear k_{obs} dependences on FNR concentration were adjusted to a two-step mechanism, given in Eq. (3) [37], to estimate minimal values of both the complex dissociation constant (K_d) and the ET rate constant (k_{et}).

$$Fd_{rd} + FNR_{ox} \overset{K_d}{\longleftrightarrow} [Fd_{rd} : FNR_{ox}] \overset{k_{et}}{\to} Fd_{ox} + FNR_{sq}. \quad (3)$$
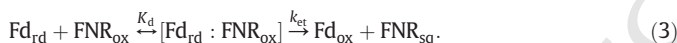
Errors in the estimated values of K_d and k_{et} were ±20% and ±10%, respectively.

2.6. Stopped-flow pre-steady-state kinetic measurements

Transient charge transfer complex (CTC) formation and HT processes between the FNR$_{hq/ox}$ variants and NADP$^+$/H were followed by stopped-flow in 50 mM Tris/HCl, pH 8.0, at 6 °C and under anaerobic conditions [14,38]. Final FNR concentrations were 25 μM, while a 25–250 μM range was used for the nucleotide. Reactions were followed by the evolution of the absorption spectra (400–1000 nm) using an Applied Photophysics SX17.MV stopped-flow equipment with a photodiode array detector (*App. Photo. Ltd.*). Typically, spectra were collected every 2.5 ms. Multiple wavelength absorption data were processed using the X-Scan software (*App. Photo. Ltd.*). Analysis of time dependent spectral changes was performed by global analysis and numerical integration methods using Pro-Kineticist (*App. Photo. Ltd.*). Data were fit to a single step model allowing estimation of the apparent conversion rate constants ($k_{A \to B}$, $k_{B \to C}$). In general, the first spectra after mixing show formation of some amount of CTC; this means a previous reaction, A → B, has occurred in the instrumental dead time (2–3 ms in our conditions), then we correlate the observed reaction with a B → C model. A, B and C are spectral species, reflecting a distribution of enzyme intermediates (reactants, CTCs, products, Michaelis-complexes) at a certain point along the reaction time course, and do not necessarily represent a single distinct enzyme intermediate. Moreover, none of them represents individual species, and their spectra cannot be included as fixed values in the global-fitting. Model validity was assessed by lack of systematic deviations from residual plots at different wavelengths,

inspection of calculated spectra and consistence among the number of significant singular values with the fit model. The apparent rate constants as a function of coenzyme concentration were globally fit to the reaction mechanisms including all the experimental data for processes in both directions (Figure S2C) [14]. In the simplest case the time-course of the reaction ($k_{A \to B}$) will be equal to the sum of the rates for the forward (k_{HT}) HT and reverse (k_{HT-1}) HT at equilibrium [14,39]. In the presence of excess of coenzyme the dependence of k_{HT} and k_{HT-1} on substrate concentration is given by standard functions for substrate saturation and competitive inhibition (inhibition constant K_i), respectively:

$$k_{A \to B} = \frac{[NADPH]k_{HT}}{[NADPH] + K_{NADPH}} + \frac{[NADP^+]k_{HT-1}}{[NADP^+] + K_{NADP^+}(1 + [NADPH]/K_i)}. \quad (4)$$

The concentration of NADP$^+$/H at equilibrium can also be estimated from the difference in the midpoint reduction potentials for NADP$^+$/H and FNR$_{ox/hq}$ redox couples (ΔE_m) and the total concentration of enzyme (E_t) (Eq. (5)):

$$\left[NADP^+ \right] = [NADPH] \frac{\left(1 + 4FNR_t \cdot 10^{\Delta E_m/29.5}/[NADPH] \right)^{1/2} - 1}{2 \cdot 10^{\Delta E_m/29.5}}. \quad (5)$$

Errors in the determination of these kinetic constants were ±15–20%.

Single-wavelength kinetic traces were recorded for accurate estimation of the hydride or deuteride transfer (HT and DT, respectively) rate constants ($k_{obsHT/HT-1}$ or $k_{obsDT/DT-1}$) in the temperature dependence assays. In these cases traces at 458 nm were recorded with the single-wavelength monochromator using the SX18.MV software (*App. Photo. Ltd.*). A 1:1 enzyme:coenzyme concentration ratio was used for these experiments using temperatures between 5.3 and 17.3 °C, since, due to the reversibility of the process, this ratio relates with the maximal experimental values for $k_{obsHT/HT-1}$ or $k_{obsDT/DT-1}$. Traces were fit to monoexponential decays to determine k_{obsHT}, $k_{obsHT-1}$, k_{obsDT} and $k_{obsDT-1}$. Errors in the determination of these kinetic constants were ±10%. The kinetic isotope effects (KIEs) were calculated as:

$$KIE = \frac{k_{obsHT}}{k_{obsDT}} \quad \text{or} \quad KIE = \frac{k_{obsHT-1}}{k_{obsDT-1}}. \quad (6)$$

Fitting the experimentally obtained rates to the Arrhenius equation allowed determining the Arrhenius pre-exponential factors (A_H and A_D) and the Activation Energy values (E_{aH} and E_{aD}). Combination of the Arrhenius equation with Eq. (6) leads to the graphical representation of the temperature dependence of the KIE.

2.7. Crystal growth, data collection and structure refinement

Crystals of S59A, Y79F and S80A AnFNR were produced under the same conditions previously reported for the WT [5,22], while those for the S80A FNR:NADP$^+$ complex were similarly obtained but without (NH$_4$)$_2$SO$_4$ and adding 1 μL of 10 mM NADP$^+$ to the drop. X-ray data sets for S59A and S80A AnFNR were collected on a Bruker-Incoatec 1 μS microfocus generator with an Axiom detector. A microstar generator with an Image Plate detector was used to collect data for Y79F FNR, whereas data for the S80A FNR:NADP$^+$ complex were collected on the ID23-1 line at ESRF (Grenoble, France). Data were processed with Proteum Suite (*Bruker*) and XDS [40] and scaled and reduced with SCALA from CCP4 [41]. All structures were solved by MOLREP [42] from CCP4, using the structures of WT AnFNR (PDB ID: 1QUE) and the AnFNR:NADP$^+$ complex (PDB ID: 1GJR) as reference models. Refinement of all structures was performed with CCP4 and COOT [43] and SFCHECK [44]. PROCHECK [45] and MOLPROBITY [46] were used to

assess final structures. S59A, Y79F and S80A FNRs diffracted up to 1.92, 2.0 and 1.9 Å, respectively, and belonged to the $P6_5$ hexagonal space group. Their V_m were 2.85, 2.86 and 2.68 Å^3/Da with one FNR molecule in their asymmetric units and 56.8, 57.0 and 53.7% solvent contents, respectively. Each model comprised residues 9-303 (S59A and Y79F FNRs) or 10-303 (S80A FNR), one FAD molecule, one SO_4^{2-} ion and water molecules. The S80A FNR:NADP$^+$ complex was solved at 2.3 Å and crystals belonged to the I4 tetragonal space group. V_m was 3.26 Å^3/Da with two molecules in the asymmetric unit and 61.93% solvent. The model included residues 9-303, one FAD, one NADP$^+$ and waters. Data for collection and refinement processes can be found in Table SP1. Coordinates and structure factors were deposited in the Protein Data Bank with accession codes 3ZBT for S59A FNR, 4BPR for Y79F FNR, 3ZBU for S80A FNR and 3ZC3 for S80A FNR:NADP$^+$.

3. Results

3.1. Interaction with partners, and oxido-reduction properties of the FNR variants

Purification of S59A, Y79F and S80A AnFNR variants produced protein yields and spectral properties (including UV–vis spectral shape, maxima position and $A_{274 nm}$/$A_{458 nm}$ ratio) similar to the WT, indicating that mutations prevented neither the assembly of FAD nor the protein folding. Nevertheless, S80A UV/vis spectral maxima slightly shifted to longer wavelengths (to 276, 397 and 466 nm), and its extinction coefficient in the flavin band-II was larger than that of WT (Fig. 2A). This suggests that Ser80 directly influences the electronic environment of the FAD isoalloxazine. Titration of the FNR$_{ox}$ variants with NADP$^+$ induced the typical difference spectra of cyanobacterial FNRs (Fig. 2B) indicative of coenzyme binding, but lacking the positive band at 509 nm detected in enzymes from plants and related with direct stacking between the NMN and the isoalloxazine [5,30,34,47]. When Ala substituted for Ser80 changes in the position and intensities of spectral features were observed with respect to WT FNR, this again suggests modification of the isoalloxazine environment (Fig. 2B) [34,48]. Saturation of the difference spectra upon increasing NADP$^+$ concentration allowed determination of $K_d^{NADP^+}$ and Δε (see Supplementary material, Figure S1). The affinity of S59A and Y79F FNR$_{ox}$s for NADP$^+$ was within a factor of two of that of WT, but decreased up to 4-fold for the S80A variant (Table 1). Altogether these observations suggest that removal of the Ser80 side-chain modifies the nicotinamide disposition into the active site. Titration of the different FNR variants with NAD$^+$ did not induce the appearance of difference spectra. This indicated that the presence of NAD$^+$ does not have any effect in the environment of the isoalloxazine ring and suggested that binding of the coenzyme is not produced, similar to that described for the WT [30,34].

Difference spectra obtained upon titration of S59A and Y79F FNR$_{ox}$ with Fd$_{ox}$ produced perturbations in the visible region very similar to those reported for the WT FNR$_{ox}$ [7], while the S80A variant showed a slight displacement of the maxima to shorter wavelengths (not shown). All the variants showed interaction parameters in the same range as for WT FNR$_{ox}$ with Fd$_{ox}$, the only exception was S59A, whose affinity for Fd$_{ox}$ increased by 3-fold (Table 1).

Photoreduction of S59A and Y79F FNRs took place following similar spectral evolution and maximal percentage of semiquinone stabilisation (ranging 16–19%) as for the WT (Fig. 2C), but reduction of the S80A variant occurred with very little semiquinone stabilisation (<4%). Due to the low degree of FNR$_{sq}$ stabilisation it was not possible to independently measure the potential for the two one-electron steps; therefore, midpoint reduction potentials for the two electron processes ($E_{ox/hq}$) were determined for all of them. $E_{ox/hq}$ for the mutants yielded values only slightly less negative (8–12 mV) than for WT AnFNR (Fig. 2D, Table 2). This was clearly the consequence of less negative $E_{sq/hq}$ values for the S59A and Y79F variants. The very little semiquinone stabilisation of S80A FNR also prevented estimation of $E_{ox/sq}$ and $E_{sq/hq}$.
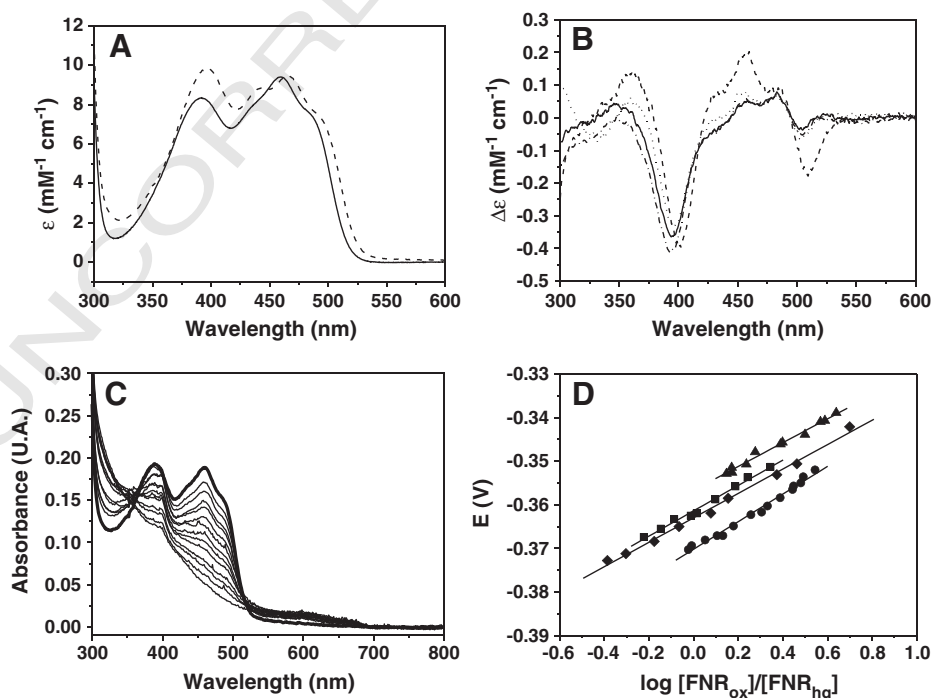
Fig. 2. Spectroscopic properties of the AnFNR variants. (A) Absorbance spectra in the visible region of WT (——) and S80A (— —) AnFNRs. (B) Difference absorbance spectra elicited upon addition of NADP$^+$ at saturating concentrations to WT (——), S59A (······), Y79F (—·—), and S80A (— —) AnFNR$_{ox}$ solutions (~20 μM). (C) Spectral evolution along step-wise photoreduction of Y79F AnFNR (20 μM). (D) Nernst plots for the reduction potential titrations of WT (●), Y79F (■), S59A (♦) and S80A (▲) AnFNRs.

Table 1
Interaction parameters for complex formation of $AnFNR_{ox}$ variants with $NADP^+$ and $AnFd_{ox}$ as determined by difference spectroscopy in 50 mM Tris/HCl, pH 8.0, at 25 °C.

FNR variant	$NADP^+$		$AnFd_{ox}$	
	K_d (μM)	$\Delta\varepsilon_{(482 - 390)}$ (mM^{-1} cm^{-1})	K_d (μM)	$\Delta\varepsilon_{(462)}$ (mM^{-1} cm^{-1})
WT	4.0	1.15	6.7	1.95
S59A	8.5	1.28[a]	2.2	1.60
Y79F	8.6	1.28	6.7	2.09
S80A	13.8	1.79[b]	6.4	3.22[c]

[a] $\Delta\varepsilon_{(458 - 396)}$.
[b] $\Delta\varepsilon_{(456 - 400)}$.
[c] $\Delta\varepsilon_{(449)}$.

3.2. Steady-state efficiency of the FNR variants

Kinetic parameters for the diaphorase activity of Y79F AnFNR reflected a very similar behaviour to the WT (Table 3). Replacement of Ser59 with Ala significantly increased the enzyme turnover (k_{cat}) with both one- and two-electron acceptors, but the effect in the catalytic efficiency only resulted relevant when using the two-electron acceptor, due to the increase in K_m^{NADPH} when using the one-electron acceptor. On the contrary, when Ser80 was substituted by Ala the catalytic efficiency decreased by 2- to 4-fold, due to a decrease in the enzyme turnover. None of the mutations improved the AnFNR ability to catalyse the DCPIP diaphorase activity using NADH as electron donor. This activity was not detected at all in the S80A variant, making it even more specific towards the phosphorylated coenzyme.

Kinetic parameters for the FNR NADPH-dependent Cyt$c$ reductase activity yielded lower k_{cat} values for the S59A and, particularly, Y79F variants with respect to WT FNR (37% and 5.5%, respectively), with unaltered K_m^{Fd} values (Table 3). No activity at all was detected for the S80A AnFNR, a fact probably related with its low ability to stabilise the semiquinone. These results indicate important deleterious effects in the ET from FNR_{hq} to Fd_{ox} by the introduced mutations.

3.3. Pre-steady-state kinetic analysis of the reduction of FNR_{ox} by Fd_{rd}

Reduction of the isoalloxazine of S59A, Y79F and S80A AnFNRs to the semiquinone state by the laser generated dRfH• followed a monoexponential absorbance decrease at 458 nm, as observed for the WT AnFNR. k_{obs} values for these reactions were linearly dependent on the FNR concentration with second-order rate constants indicating that all variants are as efficiently reduced by dRfH• as WT (Table 4) [7].

Fd/FNR ET reactions are optimised at relatively high I, as at very low salt concentrations the strong protein–protein charge interactions freeze the Fd:FNR complex in a non-optimal configuration [7]. FNR_{ox} reduction by Fd_{rd} has been here investigated in the presence of a moderately high salt concentration ($I = 120$ mM). When an excess of Fd_{ox} is additionally present in the cuvette, the laser-generated dRfH• causes its fast reduction, and a subsequent step of ET from Fd_{rd} to WT FNR_{ox} can be monitored by formation of neutral FNR_{sq} [7,12]. The FNR_{sq} formation observed at 600 nm is concomitant with Fd_{rd} oxidation, as inferred from an absorbance increase at 498 nm (an

Table 2
Midpoint reduction potentials of the AnFNR variants at 25 °C and pH 8.0[a].

FNR variant	E_m (mV)	% SQ	$E_{ox/sq}$ (mV)	$E_{sq/hq}$ (mV)
WT	−370	22	−384	−357
S59A	−364	19	−382	−346
Y79F	−363	16	−386	−340
S80A	−358	4	–	–

[a] Potentiometric titrations were carried out using 30 μM FNR, 1 μM methylviologen and benzylviologen, 2 μM dRf and 3 mM EDTA in 50 mM Tris/HCl, pH 8.0.

isosbestic point for $FNR_{ox/sq}$) in the same time frame. A similar kinetic behaviour was observed for S59A and Y79F AnFNRs. However, absorbance changes related with ET from Fd_{rd} to S80A $AnFNR_{ox}$ were detected neither at 600 nm nor at the S80A isosbestic point (500 nm), indicating that the S80A variant resulted in highly impaired accepting electrons from Fd_{rd}. At $I = 120$ mM the k_{obs} values for WT FNR_{sq} formation present a hyperbolic dependence on FNR concentration, that can be related with the formation of a transient FNR_{ox}:Fd_{rd} complex prior to the ET step (Fig. 3A). Applying the formalism previously described [37], minimal values for k_{et}, and K_d can be estimated (Table 4), which are in agreement with previously reported data [7]. The two-step model here applied to estimate K_d and k_{et} values has largely demonstrated to be extremely useful in the characterization of ET in transient protein:protein reactions [13,35–37]. This model is based in the total amount of FNR_{ox} in the sample, although under the experimental conditions used (an excess of Fd_{ox}), part of the FNR molecules would be transiently complexed with Fd_{ox}, and thus the free Fd_{rd} generated by dRfH• has to replace FNR-bound Fd_{ox}. However, it is widely accepted that, in transient protein complexes, protein association/dissociation is much faster than ET itself, and thus the ET process would be the rate limiting step rather than Fd exchange. It is worth to note that although the K_d values here described by difference spectroscopy upon titration refer to the Fd_{ox}:FNR_{ox} interaction, and the K_d values estimated by laser-flash experiments correspond to the interaction between Fd_{rd} and FNR_{ox} (which is only observable by kinetic methodology), both K_d values are of the same order of magnitude and comparable in both cases, thus supporting the validity of the kinetic models used. Regarding the kinetic properties of the FNR mutants, a similar behaviour was observed for Y79F AnFNR with k_{et} in the same range as for the WT, while the lower K_d suggested a stronger interaction between Fd_{rd} and this FNR_{ox} mutant. This later result is in agreement with the lower turnover for this variant in the Cyt$c$ reductase activity. However, a linear dependence was observed on the enzyme concentration when analysing reduction of S59A $AnFNR_{ox}$ (Fig. 3A), allowing only estimation of a bimolecular second-order rate constant (Table 4). Decreasing the I of the medium, slowed k_{obs} and induced a hyperbolic dependence on FNR concentration (Fig. 3A, Table 4). This indicates the formation of a transient complex between S59A FNR_{ox} and Fd_{rd} at lower I, while more physiological salt concentrations make the system shift to a collisional ET mechanism. Changes in the concentration profile dependence have also been reported for the WT enzyme at different Is (Fig. 3A, Table 4) [49].

The influence of I on the Fd/FNR interaction was further analysed to investigate the effects induced by the mutations on the electrostatics of the interaction. Biphasic dependences of k_{obs} with increasing NaCl concentration were observed with the WT, S59A and Y79F variants (Fig. 3B), despite the fact that for S59A FNR the k_{obs} maximum is shifted to higher I. The S80A variant did not show however significant reactivity at any salt concentration (not shown). The bell-shaped profile for the dependence of k_{obs} with I is related with the re-arrangement of the initial FNR_{ox}:Fd_{rd} interaction to achieve the optimal ET conformation, indicating the occurrence of protein–protein dynamic motions that are blocked by strong electrostatic interactions at very low I [7].

3.4. Transient kinetics of the hydride transfer reactions between FNR and the coenzyme. Kinetic isotopic effect (KIE) and dependence of the temperature

Stopped-flow analysis of the transient HT processes between S59A $FNR_{hq/ox}$ and $NADP^+$/H followed very similar patterns to those reported for the WT enzyme: fast formation of two intermediate CTCs prior and after the HT event, whatever the direction of the reaction (CTC-1 and CTC-2, characterised by spectral bands centred at 600 nm and 800 nm, respectively (Figure S2)) [4,14,16,38]. Similar to the WT system, evolution of the initial CTC species for S59A also started in the instrumental dead time (Fig. 4A and D), but a slight increase in k_{HT} can be envisaged

Table 3

Steady-state kinetic parameters of the different AnFNR variants for the diaphorase (with either DCPIP or ferricyanide as electron acceptors) and cytochrome c reductase activities in 50 mM Tris/HCl, pH 8.0 at 25 °C.

FNR variant	DCPIP diaphorase						Fe(CN)$_6^{3-}$ diaphorase			Cytochrome c reductase		
	NADPH			NADH			NADPH					
	K_m^{NADPH} (μM)	k_{cat} (s^{-1})	k_{cat}/K_m (μM^{-1} s^{-1})	K_m^{NADH} (μM)	k_{cat} (s^{-1})	k_{cat}/K_m (μM^{-1} s^{-1})	K_m^{NADPH} (μM)	k_{cat} (s^{-1})	k_{cat}/K_m (μM^{-1} s^{-1})	K_m^{Fd} (μM^{-1})	k_{cat} (s^{-1})	k_{cat}/K_m (μM^{-1} s^{-1})
WT	6.0	81.5	13.6	800	0.16	$2.0.10^{-4}$	11	370	34	1	176	176
S59A	5.3	146.0	27.5	990	0.56	$5.6.10^{-4}$	42	1000	24	0.99	65.7	66
Y79F	3.8	73.0	19.2	640	0.21	$3.3.10^{-4}$	13.6	304	22	1.16	9.6	8.3
S80A	4.6	30.4	6.6	n.d.[a]	n.d.[a]	n.d.[a]	7.2	93.4	13	n.d.[a]	n.d.[a]	n.d.[a]

[a] Activity was not detected.

for this variant with respect to WT (Table 5). Replacements at Tyr79 and Ser80 produced more evident effects (Fig. 4, Table 5). A decrease in the amplitude of the spectral band for CTC-2 was observed upon reduction of Y79F FNR$_{ox}$ by NADPH, while HT was slightly hampered in both directions (Fig. 4B and E, Table 5). More drastic effects were observed when Ala substituted for Ser80. Reduction of S80A FNR$_{ox}$ by NADPH occurred without spectral CTC-2 stabilisation (Fig. 4C), and no spectral features of CTC at all were detected for the reverse reaction (Fig. 4F). Additionally, both reactions showed less than 5% of the WT efficiency in HT (Table 5).

Due to the reversibility of the process producing the apparent decrease in the experimentally measured rate constants upon increasing coenzyme concentration and to the k_{HT} and k_{HT-1} rates being in close to the instrumental detection limit for some variants, equimolecular concentrations of enzyme and coenzyme, as well as the use of the single-wavelength detector, were selected to further investigate this mechanism by analysing KIEs on the HT processes. The main observable difference between HT and DT processes was the considerable decrease in k_{obsDT} and $k_{obsDT-1}$ values with respect to the corresponding k_{obsHT} and $k_{obsHT-1}$ ones for all the FNR variants (Fig. 5A and B, Table 6), therefore, inducing moderate to important KIEs. For each particular variant the KIE was slightly larger for the reduction of FNR$_{ox}$ by the coenzyme than for the reverse reaction. KIEs for the S59A and Y79F variants were in the same range as for WT, but processes with S80A FNR showed considerably larger KIEs (up to 6-fold for the FNR reductive process). k_{obs} values for the reduction of the different FNR$_{ox}$ forms by NADPH and NADPD, as well as for the reverse processes, resulted highly dependent on temperature (Fig. 5A and B), indicating high activation energies (E_a) (Table 6), particularly for the reaction of S80A FNR$_{ox}$ with NADPD. The obtained parameters were evaluated within the environmentally coupled tunnelling model that distinguishes between two dynamics contributions to the protein motion: active (or gating) and passive (environmental reorganisation) [50–53]. Arrhenius plots for the HT and DT reactions of WT, S59A and Y79F FNRs corresponded to two almost parallel straight lines (Fig. 5A and B), which produced an almost temperature-independent KIE in the assayed range (Fig. 5C and D). In the reactions of WT FNR, the moderate KIEs and Arrhenius pre-exponential factors ratios (A_H/A_D and A_{H-1}/A_{D-1} just above

Table 4

Rate constants for the laser-flash induced reduction of the AnFNR$_{ox}$ variants by dRf and AnFd.

FNR variant	Reduction by dRfH[a]	Reduction by AnFd[b]		
	k_2 (M^{-1} s^{-1})	k_2 (M^{-1} s^{-1})	k_{et} (s^{-1})	K_d (μM)
WT	2.3×10^8	3.0×10^{7a}	7780	17.0
S59A	3.5×10^8	2.5×10^8	7100[c]	26.0[c]
Y79F	3.5×10^8		10,870	4.0
S80A	2.2×10^8		–	–

[a] Reaction in 4 mM phosphate, pH 7.0 ($I = 20$ mM).
[b] Reaction in 4 mM phosphate, pH 7.0 at 100 mM NaCl ($I = 120$ mM), unless otherwise stated.
[c] Reaction in 4 mM phosphate, pH 7.0 at 20 mM NaCl ($I = 40$ mM).

unity), together with the high E_a and small ΔE_a, were interpreted as mainly tunnelling of the light isotope and contribution of both the environmental reorganisation (passive) and the vibrationally enhanced modulation (gating) to the tunnel reaction [14,54]. A similar behaviour might be predicted for S59A and Y79F FNRs in their non-photosynthetic reactions, with an apparent more predominant gating contribution, indicated by their slightly larger and lower, respectively, ΔE_a and A_H/A_D values. Backward processes for these two variants showed slightly lower KIEs that were temperature-independent (Fig. 5C and D), ΔE_a close to zero and larger A_{H-1}/A_{D-1} values with respect to the WT (Table 6). Altogether these parameters appear consistent with environmental heavy atom reorganisation contributing to the tunnel for the reaction of S59A and Y79F FNR$_{ox}$ with NADPH/D, and almost no gating contribution. Reduction of NADP$^+$ by S80A FNR$_{hq}$ behaved similarly to S59A and Y79F FNRs, but with larger KIE and A_H/A_D ratio, suggesting that a full tunnelling passive dynamics model with protein environmental reorganisation dominates the HT (without gating contribution). The most striking results were observed for reduction of S80A FNR$_{ox}$ by the coenzyme. This reaction occurred with a large KIE that considerably decreased with temperature (Fig. 5C), as consequence of a large E_{aD} that also produced a considerable increase in ΔE_a. This, together with the much lower than unity A_H/A_D, suggests that vibrationally enhanced modulation of the tunnel probability (gating or active dynamics) is dominating this reaction [50–53].

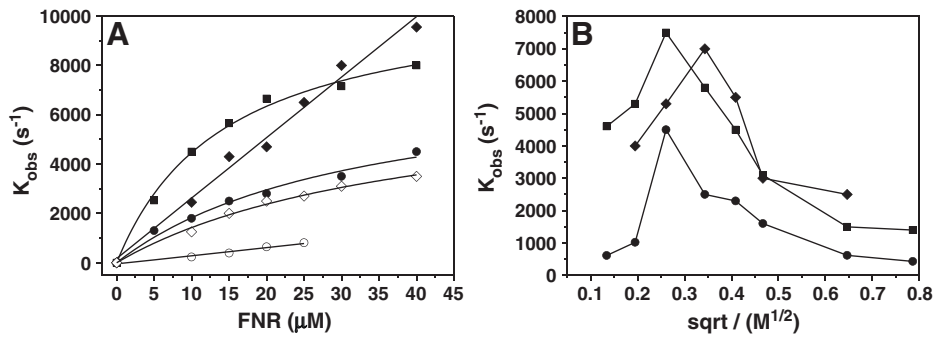### 3.5. The structural environment of the mutated positions

S59A, Y79F and S80A FNR$_{ox}$s showed overall crystal structures similar to that of WT (r.m.s.d. ~0.26 on Cα atoms aligned for all of them). Mutations did not lead to significant modification of the FAD isoalloxazine environment and were constricted to the interactions involving the modified side-chains (Fig. 6A). The larger differences resulted in the loop 105–111, flexible in all AnFNR structures so far described and suggested to accommodate the adenosine moiety of the FAD [21,22,55]. Y79F FNR showed the highest B factors for the residues contained in this loop; from 103 to 114 the B factor is higher than 40 Å^2 (being its overall B factor of 21.54 Å^2). This might be due to the fact that the cofactor is not engaged through its ribityl motif with this residue and no water molecule is mimicking the removed hydroxyl group. Ala substitution for Ser59 provoked removal of two defined water molecules that interact with the OG atom of Ser59 and with the OE1 atom of Glu301, respectively, in WT FNR. Besides this, the FAD environment, especially the H-bond network involving Ser80 and Glu301, is not much affected by the mutation. Changes in the S80A FNR crystal structure are restricted to the H-bonds involving the removed hydroxyl group. Ala80 cannot H-bond the side-chain of Glu301, being only in contact with N5i through a H-bond with its main chain N. Again, no water molecule mimics the H-bond network established by the Ser80 side-chain. The highly conserved water molecule, proposed to act as a proton donor to the N5i of FAD, is found in the S80A FNR structure, as in that of WT, interacting with the hydroxyl of Tyr303, but it is at closer distance with the O4 atom of FAD (2.9 Å) than in the WT structure (3.17 Å)

Fig. 3. Laser-flash induced transient kinetic analysis for the reduction of the AnFNR$_{ox}$ variants by AnFd$_{rd}$. (A) Dependence of k_{obs} on FNR concentration for the reduction by Fd$_{rd}$ of WT (○) FNR$_{ox}$ at I = 20 mM, and of WT (●), Y79F (■) and S59A (♦) FNR$_{ox}$ at I = 120 mM, and of S59A (◊) FNR$_{ox}$ at I = 40 mM. Reaction mixtures contained 40 μM Fd$_{ox}$. (B) Dependence of k_{obs} on the square root of I for the reduction of WT (●), Y79F (■) and S59A (♦) FNR$_{ox}$ by Fd$_{rd}$. Reaction mixtures contained 40 μM Fd$_{ox}$ and 30 μM FNR$_{ox}$.
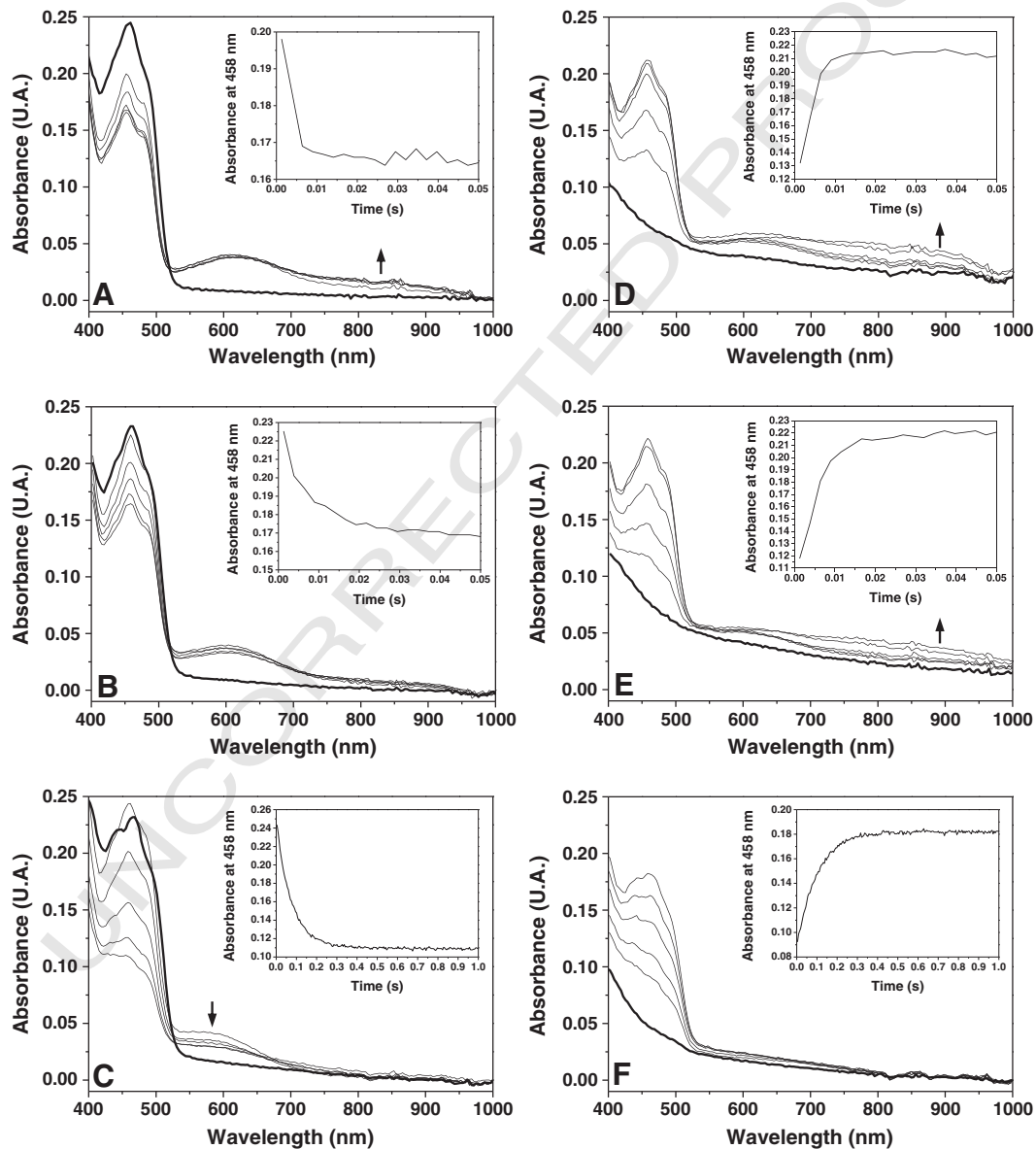
Fig. 4. Spectral evolution along the HT processes between AnFNR and the coenzyme followed by stopped-flow. Reduction by NADPH of (A) S59A FNR$_{ox}$ (spectra recorded at 1.28, 3.84, 6.4, 8.96 and 49.92 ms after mixing), (B) Y79F FNR$_{ox}$ (spectra recorded at 1.28, 3.84, 8.96, 24.32 and 49.92 ms), and (C) S80A FNR$_{ox}$ (spectra recorded at 3.84, 29.4, 80.6, 157.4 and 997.1 ms). Reoxidation by NADP$^+$ of photoreduced (D) S59A FNR$_{hq}$ (spectra recorded at 1.28, 3.84, 6.4, 8.96 and 49.92 ms), (E) Y79F FNR$_{hq}$ (spectra recorded at 1.28, 3.84, 8.96, 19.2 and 49.92 ms) and (F) S80A FNR$_{hq}$ (spectra recorded at 3.84, 29.4, 80.6, 157.4 and 997.1 ms). In all cases the thick line is the spectrum of the oxidised (for A, B and C) or reduced (D, E and F) protein before mixing. Insets show the time evolution of the absorption at 458 nm. Reactions were carried out with FNR at ~25 μM and coenzyme ~100 μM final concentrations in 50 mM Tris/HCl pH 8.0 at 6 °C.

	FNR$_{ox}$ and NADPH	FNR$_{hq}$ and NADP$^+$
FNR variant	k_{HT1} (s^{-1})	k_{HT-1} (s^{-1})
WT[a]	300	285
S59A	390	253
Y79F	122.6	186
S80A	13.2	10.1

t5.10 [a] Data from [14].

(Fig. 6A). Another common characteristic in these structures, and in contrast with the WT, is the orientation of Arg264 towards the C-terminal, its guanidinium H-bonding the C-terminal carboxylate of Tyr303 (Fig. 6A). This interaction was already predicted by MD simulations [15] and does not appear related with the introduced mutations, further suggesting a contribution for Arg264 in the displacement of Tyr303 to trigger the entrance of the nicotinamide into the catalytic site.

Finally, in the S80A FNR:NADP$^+$ complex, the N atom of Ala80 H-bonds N5i and O4i. In this structure, NADP$^+$ binds in a similar unproductive conformation to that previously reported for WT [22], although the isoalloxacine-Tyr303 rings stacking distance gets slightly larger (around 0.4 Å) and the nicotinamide lies slightly closer to Tyr303, bridging its N7n atom and the OH of Tyr303.

4. Discussion

Here we show that replacement of Ser59 with Ala improved the catalytic efficiency of the diaphorase activity of AnFNR (particularly the k_{cat}) with respect to the WT, as consequence of increasing the k_{HT}

(Tables 3 and 5). This mutation also influences the affinity between FNR and Fd as a function of their oxido-reduction states and of the I of the media (Tables 1 and 4, Fig. 3). Thus, despite steady-state and pre-steady-state kinetics indicate that S59A FNR$_{ox}$ is able to efficiently receive electrons from Fd$_{rd}$ (the photosynthetic process) once the interaction is formed, its differential behaviour dependence on the ionic strength with respect to the WT indicates that the mutation influences the electrostatic and hydrophobic contributions to produce the most productive complex for ET (Table 4, Fig. 3) [56]. Moreover, the introduced mutation particularly favours the non-photosynthetic HT from NADPH to FNR$_{ox}$, as well as the ET from Fd$_{rd}$, particularly at higher ionic strengths than for the WT. This might correlate with the $E_{sq/hq}$ of the variant being slightly less negative. Additionally, KIE analyses for the reactions of S59A FNR with the coenzyme (Fig. 5, Table 6) suggest larger contribution of the vibrationally enhanced modulation to the tunnel reaction during HT for the reduction of the protein by the coenzyme. These data indicate higher flexibility at the active site environment for the non-photosynthetic process along the reaction coordinate for S59A FNR, regarding both its photosynthetic reaction and the WT behaviour. Therefore, Ser59 indirectly modulates the geometry of the active site, the interaction with substrates and the electronic properties of the isoalloxazine ring, and in consequence the ET and HT processes. Altogether these data support the hypothesis derived from MD studies on AnFNR [15], and confirm that the side-chain of Ser59 indirectly modulates the architecture of the reactive complexes during both ET with Fd and HT with the coenzyme.

Previous substitutions at Tyr89 in *Pisum sativum* FNR (Tyr79 in AnFNR) with Ser or Glu led to fatal consequences in terms of protein stability and FAD binding, while replacements by Phe and Trp considerably reduced the catalytic efficiency and affinity for the coenzyme [8]. On the contrary, replacement of Tyr79 by Phe in AnFNR only slightly modulated the binding and diaphorase activity parameters with the coenzyme, as
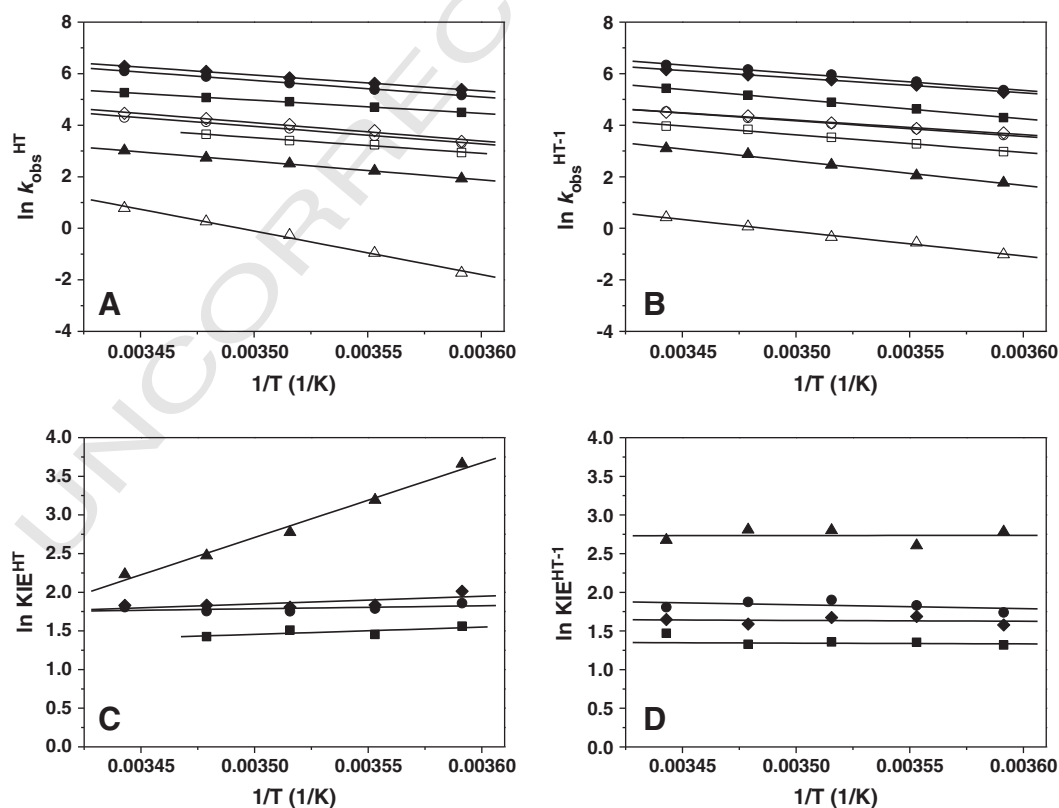
Fig. 5. Temperature dependence of the HT rates and KIEs. Arrhenius plots ($\ln k_{obs} = \ln A - E_a / RT$) of the kinetic data for the reactions of (A) FNR$_{ox}$ with NADPH (closed symbols) or NADPD (open symbols) and of (B) FNR$_{hq}$ or D-FNR$_{hq}$ (open symbols) with NADP$^+$ (closed symbols). Temperature dependence of the KIEs for (C) FNR$_{ox}$ reduction and (D) FNR$_{hq}$ reoxidation by the coenzyme. Data correspond to WT (●), S59A (♦), Y79F (■), and S80A (▲) AnFNRs.

Table 6

KIEs for the HT processes catalysed by the different AnFNR variants.

FNR variant	HT (FNR$_{ox}$ + NADPH)			DT (FNR$_{ox}$ + NADPD)			KIE[a]	ΔE_a $E_{aD} - E_{aH}$ (kcal mol^{-1})	A_H/A_D
	k_{obsHT}[a] (s^{-1})	E_{aH} (kcal mol^{-1})	A_H (s^{-1})	k_{obsDT}[a] (s^{-1})	E_{aD} (kcal mol^{-1})	A_D (s^{-1})			
WT[c]	175	12.8	1.8×10^{12}	27	13.5	1.2×10^{12}	6.4	0.7	1.5
S59A	212	12.2	8.2×10^{11}	29.2	14.2	4.2×10^{12}	7.5	2.0	0.2
Y79F	90	10.2	9.1×10^{9}	19	12.1	6.4×10^{10}	4.8	1.9	0.14
S80A	6.8	14.4	1.3×10^{12}	0.17	33.5	4.2×10^{25}	39[b]	19.2	3×10^{-14}

	HT-1 (FNR$_{hq}$ + NADP$^+$)			DT-1 (D-FNR$_{hq}$ + NADP$^+$)				ΔE_{a-1}	
	$k_{obsHT-1}$[a] (s^{-1})	E_{aH-1} (kcal mol^{-1})	A_{H-1} (s^{-1})	$k_{obsDT-1}$[a] (s^{-1})	E_{aD-1} (kcal mol^{-1})	A_{D-1} (s^{-1})	KIE[a]	$E_{aD-1} - E_{aH-1}$ (kcal mol^{-1})	A_{H-1}/A_{D-1}
WT[c]	229	11.6	3.2×10^{11}	37	12.1	1.1×10^{11}	5.7	0.5	2.8
S59A	196	11.5	2.0×10^{11}	40.5	11.2	2.6×10^{10}	4.8	−0.2	7.5
Y79F	73	15.1	5.0×10^{13}	19.7	15.0	1.3×10^{13}	3.7	−0.1	3.8
S80A	5.8	18.7	2.8×10^{15}	0.36	18.4	1.1×10^{14}	16.1	−0.3	15

[a] Values obtained in a stopped-flow equipment at 5.3 °C and with equimolecular concentrations of protein and coenzyme. Evolution of the reaction was followed at the single wavelength of 458 nm.

[b] Temperature dependent KIEs.

[c] Data from [14].

well as the stabilisation of CTCs during HT, being major changes reduced to a decrease in k_{HT1} and k_{HT-1} within 2-fold regarding the WT (Tables 1, 3, 5 and 6). Regarding Fd, the mutation increases the affinity of the Fd$_{rd}$: FNR$_{ox}$ complex and the ET rate between them (Table 4), while the reverse ET appears considerably hindered (Table 3). These effects with Fd might relate with the slightly less negative midpoint reduction potential of the variant, particularly $E_{sq/hq}$, that will favour its reduction regarding the WT (Table 2). Therefore, altogether the observed effects suggest that the H-bond between the hydroxyl group of Tyr79 and the ribityl portion of the cofactor, despite not being critical for ET and HT, indirectly contributes to the reactivity in productive complexes. These data agree with previous mutations in the Lys75–Leu78 peptide, where side-chains, despite not being in direct contact with the isoalloxazine ring, have been shown to slightly displace its midpoint reduction potentials to less negative values [57,58]. Thus, Tyr79 can be included among the side-chains tuning the flavin midpoint potential by creating a defined environment that modulates the FAD conformation.

The last residue here analysed, Ser80, is a key one in the active site of plastidic type FNRs where together with Cys261 and Glu301, it constitutes a highly conserved catalytic triad (Fig. 1A) [2,27,28]. Its main-chain directly H-bonds the isoalloxazine N5i atom as well as the O4i atom via a conserved water molecule, while its hydroxyl interacts with another conserved water molecule that H-bonds Glu301, Tyr303, and N5i (Fig. 6A) [21,59]. Mutations at the equivalent position in spinach leaves FNR, Ser96, [11] impaired catalysis for the S96V and S96G variants with respect to the WT, while it was not possible to produce the S96A variant. We have succeeded in producing the S80A mutant in AnFNR. This replacement slightly modifies the electronic environment of the FAD isoalloxazine ring regarding the WT, and has a deleterious effect in its semiquinone stabilisation (Fig. 2), suggesting that this later process is finely controlled by the H-bond network involving Ser80, Glu301, Tyr303 and N5i. This observation is also consistent with the mutant lacking the ability to accept a single electron from Fd$_{rd}$ in the Fd-mediated laser-flash induced ET experiments as well as to donate a single electron to Fd$_{ox}$ in the Cytc reductase assay, given the formation of the FNR$_{sq}$ intermediate is necessary for both reactions. Noticeably, the S80A mutant shows a similar decrease in efficiency, regarding de WT, in the diaphorase assay when using either one-electron or two-electron acceptors. This suggests that the nature of the small, non-specific and non-physiological collisional K$_3$Fe(CN)$_6$ one-electron acceptor allows it to extract a single electron from S80A FNR$_{hq}$ through the reduce amount of semiquinone that this mutant stabilizes (Table 2). On the contrary, processes with Fd include complex formation and dissociation rate limiting steps that modify FNR midpoint

reduction potentials [13]. The results here present suggest that in the case of S80A FNR interaction with Fd further decreases the low stability of its semiquinone. Regarding the coenzyme the mutation produced minor effects in its affinity. Despite the fact that its E_m, slightly less negative than in WT (Table 2), would apparently favour HT events from the coenzyme, we observed important deleterious effects in turnover, catalytic efficiency, HT rate constants, and the stabilisation of CTCs during the HT event for both the forward and reverse HT reactions (Fig. 4, Tables 3 and 5). All these data are in agreement with those reported for the Ser96 mutants in spinach FNR [11], further indicating that this Ser is critical to generate the architecture of the catalytically competent complex upon coenzyme binding in both the cyanobacterial and plant enzymes. Since the structures obtained for mutants at this Ser (both in AnFNR (Ser80) and the spinach enzyme (S96)) only show changes in the H-bond network involving this position (Fig. 6A), this network must be critical for the efficiency of the HT process. In agreement with this conclusion previous MD simulations suggested that the Ser80 side-chain might contribute to fix the position of the amide of NADP$^+$ and, as consequence, the position of the nicotinamide ring in the active site cavity [15]. The contribution of the Ser80 side-chain to the optimal architecture of the catalytically competent complex between FNR and the coenzyme is here further supported by the analysis of the active site dynamics during the HT event (Fig. 5 and Table 6). HT and DT reactions for WT FNR, in both the forward and reverse directions, have been explained applying a tunnelling model in which both environmental reorganisation (passive dynamics) and vibrational enhancement (active dynamics) contribute to the reaction [14,16]. However, KIE analyses for the processes of the S80A FNR mutant best fitted to the two extreme cases in which the tunnelling reaction is completely dominated by either environmental reorganisation or vibrational enhancement [60]. Thus, reduction of S80A FNR$_{ox}$ by NADPH/D was consistent with a full tunnelling model in which vibrational fluctuations of the active site (gating) are able to compress the hydrogen donor–acceptor distance during the HT event, making tunnelling more probable (specially for the light isotope) as long as the temperature increases. On the contrary, parameters measured for the oxidation of S80A FNR$_{hq}$ by NADP$^+$ suggest no gating contribution to the HT event, being the initial environmental thermal reorganisation of the whole active site the only dynamics contribution controlling the process. Therefore, modifications on the H-bond network caused by substitution of Ser80 with alanine entail important perturbations on the flexibility of the active site of FNR along the HT reaction coordinate. In the case of the reaction of S80A FNR$_{ox}$ with NADPH, the organisation of the close environment of the donor (C4n) and acceptor (N5i) atoms allows them to undergo
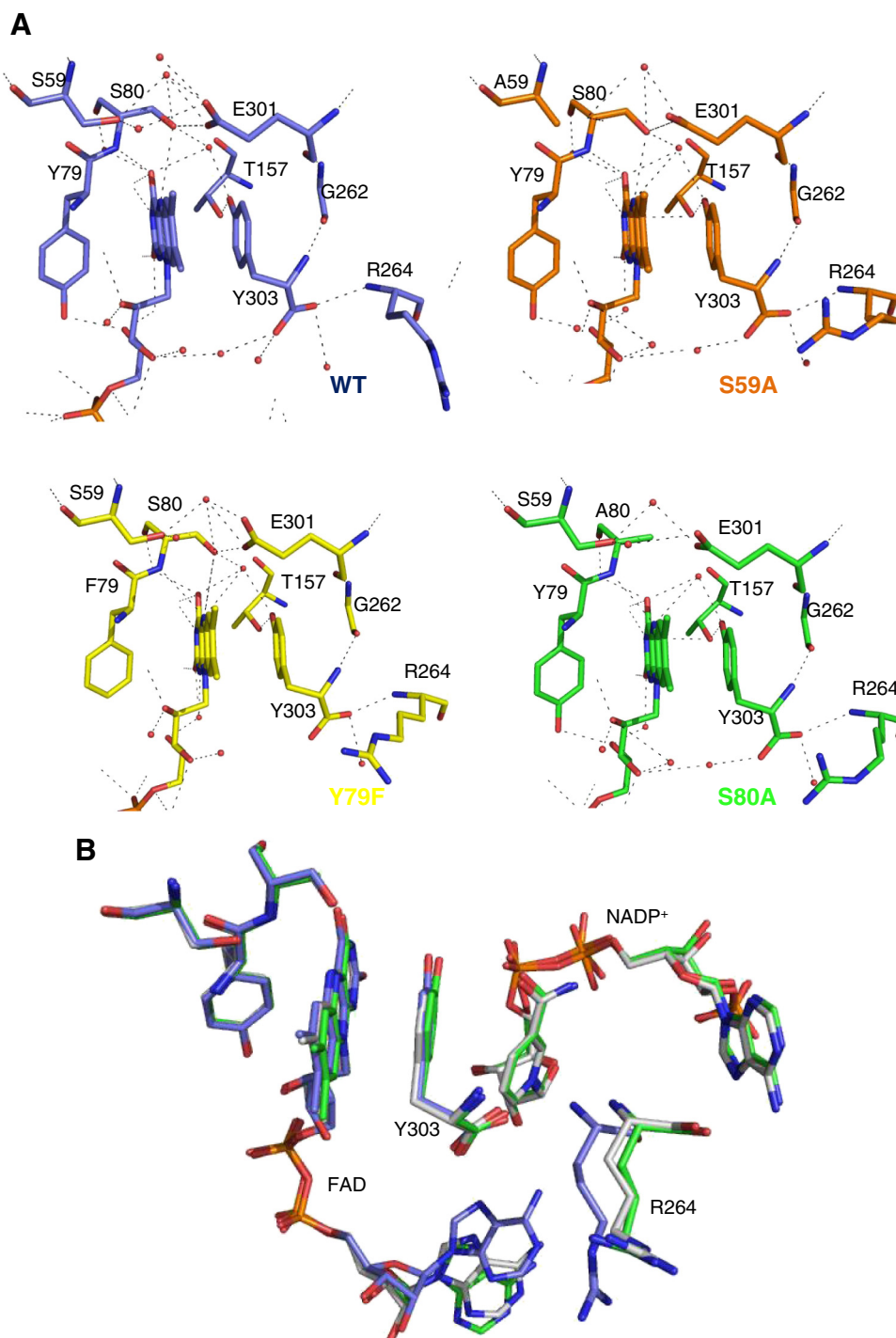
Fig. 6. Influence of the mutations in the active site geometry of AnFNR. (A) H-bond network at the active sites of the WT FNR (C in blue, PDB ID: 1QUE), S59A FNR (C in orange), Y79F FNR (C in yellow) and S80A FNR (C in green) crystal structures. Residues involved in the interactions are drawn in sticks. (B) Superposition of the actives sites of WT FNR (C in white, PDB ID: 1QUE), the WT FNR:NADP+ complex (C in blue, PDB ID: 1GJR) and the S80A FNR:NADP+ complex (C green).

important vibrational fluctuations to attain the optimal distance and orientation for efficient HT. On the contrary, for the reverse reaction, once the NADP+ nicotinamide reaches the active site of S80A FNR$_{hq}$ the reduced isoalloxazine and oxidised nicotinamide rings remain "frozen", without any further flexibility of the active site contributing to improve its relative distance and orientation to reach the hydrogen tunnelling ready conformation. Therefore, the S80A mutation highly compromises the active site environment fluctuations required in FNR to increase the HT probability, producing important thermodynamic and kinetic consequences in the process that are reflected in the enzyme efficiency, mechanism and reversibility of the process, all of them particular facts of plant type FNRs. Altogether these data confirm the importance of Ser80 in both the ET and HT processes, adding information about its roles. Thus, this Ser side-chain modulates the midpoint reduction potential of the flavin ring and contributes to the stabilisation of its semiquinone state, a key factor for efficient ET exchange between FNR and Fd. Additionally, it also contributes to stabilise the nicotinamide ring in the optimal

geometric conformation regarding the isoalloxazine ring for an efficient HT event through a tunnelling process following similar dynamics for both the photosynthetic and non-photosynthetic reactions, thus ensuring the efficiency and reversibility of the process.

In conclusion, as new information becomes available additional roles might be envisaged for residues in the active site of FNR. Among these residues are Tyr79 and Ser80, previously analysed in FNRs from higher plants [8,11,26]. Additionally, other residues not considered previously, such as Ser59, might indirectly contribute to the efficiency of the HT with the coenzyme by modulating the architecture of the reactive complexes [15]. Here, we present proofs for the implication of H-bond connections between the flavin and the polypeptide chain, direct or via water molecules, in the FNR catalytic efficiency, showing that the isoalloxazine environment strongly influences FAD_{sq} stabilisation and ET from Fd. Moreover, an additional key role is predicted for Ser80 during the HT step providing optimal active site geometry, including not only the final disposition between the reacting N5Hi and C4n atoms but also the active site motions required to achieve it.

Acknowledgements

Appendix A. Supplementary data

Supplementary data to this article can be found online at http://dx.doi.org/10.1016/j.bbabio.2013.10.010.

References

[1] M. Medina, Structural and mechanistic aspects of flavoproteins: photosynthetic electron transfer from photosystem I to NADP+, FEBS J. 276 (2009) 3942–3958.

[2] A. Aliverti, V. Pandini, A. Pennati, M. de Rosa, G. Zanetti, Structural and functional diversity of ferredoxin-NADP+ reductases, Arch. Biochem. Biophys. 474 (2008) 283–291.

[3] E.A. Ceccarelli, A.K. Arakaki, N. Cortez, N. Carrillo, Functional plasticity and catalytic efficiency in plant and bacterial ferredoxin-NADP(H) reductases, Biochim. Biophys. Acta 1698 (2004) 155–165.

[4] C.J. Batie, H. Kamin, Electron transfer by ferredoxin:NADP+ reductase. Rapid-reaction evidence for participation of a ternary complex, J. Biol. Chem. 259 (1984) 11976–11985.

[5] J. Tejero, I. Pérez-Dorado, C. Maya, M. Martínez-Júlvez, J. Sanz-Aparicio, C. Gómez-Moreno, J.A. Hermoso, M. Medina, C-terminal tyrosine of ferredoxin-NADP+ reductase in hydride transfer processes with NAD(P)+/H, Biochemistry 44 (2005) 13477–13490.

[6] M.A. Musumeci, A.K. Arakaki, D.V. Rial, D.L. Catalano-Dupuy, E.A. Ceccarelli, Modulation of the enzymatic efficiency of ferredoxin-NADP(H) reductase by the amino acid volume around the catalytic site, FEBS J. 275 (2008) 1350–1366.

[7] M. Medina, M. Martínez-Júlvez, J.K. Hurley, G. Tollin, C. Gómez-Moreno, Involvement of glutamic acid 301 in the catalytic mechanism of ferredoxin-NADP+ reductase from Anabaena PCC 7119, Biochemistry 37 (1998) 2715–2728.

[8] A.K. Arakaki, E.G. Orellano, N.B. Calcaterra, J. Ottado, E.A. Ceccarelli, Involvement of the flavin si-face tyrosine on the structure and function of ferredoxin-NADP+ reductases, J. Biol. Chem. 276 (2001) 44419–44426.

[9] A. Aliverti, T. Lubberstedt, G. Zanetti, R.G. Herrmann, B. Curti, Probing the role of lysine 116 and lysine 244 in the spinach ferredoxin-NADP+ reductase by site-directed mutagenesis, J. Biol. Chem. 266 (1991) 17760–17763.

[10] A. Aliverti, L. Piubelli, G. Zanetti, T. Lubberstedt, R.G. Herrmann, B. Curti, The role of cysteine residues of spinach ferredoxin-NADP+ reductase as assessed by site-directed mutagenesis, Biochemistry 32 (1993) 6374–6380.

[11] A. Aliverti, C.M. Bruns, V.E. Pandini, P.A. Karplus, M.A. Vanoni, B. Curti, G. Zanetti, Involvement of serine 96 in the catalytic mechanism of ferredoxin-NADP+ reductase: structure–function relationship as studied by site-directed mutagenesis and X-ray crystallography, Biochemistry 34 (1995) 8371–8379.

[12] I. Nogués, J. Tejero, J.K. Hurley, D. Paladini, S. Frago, G. Tollin, S.G. Mayhew, C. Gómez-Moreno, E.A. Ceccarelli, N. Carrillo, M. Medina, Role of the C-terminal tyrosine of ferredoxin-nicotinamide adenine dinucleotide phosphate reductase in the electron transfer processes with its protein partners ferredoxin and flavodoxin, Biochemistry 43 (2004) 6127–6137.

[13] J.K. Hurley, R. Morales, M. Martínez-Júlvez, T.B. Brodie, M. Medina, C. Gómez-Moreno, G. Tollin, Structure–function relationships in Anabaena ferredoxin/ferredoxin-NADP+ reductase electron transfer: insights from site-directed mutagenesis, transient absorption spectroscopy and X-ray crystallography, Biochim. Biophys. Acta 1554 (2002) 5–21.

[14] J.R. Peregrina, A. Sánchez-Azqueta, B. Herguedas, M. Martínez-Júlvez, M. Medina, Role of specific residues in coenzyme binding, charge-transfer complex formation, and catalysis in Anabaena ferredoxin-NADP+ reductase, Biochim. Biophys. Acta 1797 (2010) 1638–1646.

[15] J.R. Peregrina, I. Lans, M. Medina, The transient catalytically competent coenzyme allocation into the active site of Anabaena ferredoxin-NADP+ reductase, Eur. Biophys. J. (2012).   Q19

[16] I. Lans, J.R. Peregrina, M. Medina, M. García-Viloca, A. González-Lafont, J.M. Lluch, Mechanism of the hydride transfer between Anabaena Tyr303Ser FNR$_{rd}$/FNR$_{ox}$ and NADP+/H. A combined pre-steady-state kinetic/ensemble-averaged transition-state theory with multidimensional tunneling study, J. Phys. Chem. B 114 (2010) 3368–3379.

[17] Z. Deng, A. Aliverti, G. Zanetti, A.K. Arakaki, J. Ottado, E.G. Orellano, N.B. Calcaterra, E.A. Ceccarelli, N. Carrillo, P.A. Karplus, A productive NADP+ binding mode of ferredoxin-NADP+ reductase revealed by protein engineering and crystallographic studies, Nat. Struct. Biol. 6 (1999) 847–853.

[18] I. Lans, M. Medina, E. Rosta, G. Hummer, M. García-Viloca, J.M. Lluch, A. González-Lafont, Theoretical study of the mechanism of the hydride transfer between ferredoxin-NADP+ reductase and NADP+: the role of Tyr303, J. Am. Chem. Soc. 134 (2012) 20544–20553.

[19] P.A. Karplus, C.M. Bruns, Structure–function relations for ferredoxin reductase, J. Bioenerg. Biomembr. 26 (1994) 89–99.

[20] M. Ingelman, S. Ramaswamy, V. Niviere, M. Fontecave, H. Eklund, Crystal structure of NAD(P)H:flavin oxidoreductase from Escherichia coli, Biochemistry 38 (1999) 7040–7049.

[21] L. Serre, F.M. Vellieux, M. Medina, C. Gómez-Moreno, J.C. Fontecilla-Camps, M. Frey, X-ray structure of the ferredoxin:NADP+ reductase from the cyanobacterium Anabaena PCC 7119 at 1.8 Å resolution, and crystallographic studies of NADP+ binding at 2.25 Å resolution, J. Mol. Biol. 263 (1996) 20–39.

[22] J.A. Hermoso, T. Mayoral, M. Faro, C. Gomez-Moreno, J. Sanz-Aparicio, M. Medina, Mechanism of coenzyme recognition and binding revealed by crystal structure analysis of ferredoxin-NADP+ reductase complexed with NADP+, J. Mol. Biol. 319 (2002) 1133–1142.

[23] M.B. Murataliev, R. Feyereisen, F.A. Walker, Electron transfer by diflavin reductases, Biochim. Biophys. Acta 1698 (2004) 1–26.

[24] C.C. Correll, C.J. Batie, D.P. Ballou, M.L. Ludwig, Phthalate dioxygenase reductase: a modular structure for electron transfer from pyridine nucleotides to [2Fe–2S], Science 258 (1992) 1604–1610.

[25] C.C. Correll, M.L. Ludwig, C.M. Bruns, P.A. Karplus, Structural prototypes for an extended family of flavoprotein reductases: comparison of phthalate dioxygenase reductase with ferredoxin reductase and ferredoxin, Protein Sci. 2 (1993) 2112–2133.

[26] A. Aliverti, Z. Deng, D. Ravasi, L. Piubelli, P.A. Karplus, G. Zanetti, Probing the function of the invariant glutamyl residue 312 in spinach ferredoxin-NADP+ reductase, J. Biol. Chem. 273 (1998) 34008–34015.

[27] V.I. Dumit, T. Essigke, N. Cortez, G.M. Ullmann, Mechanistic insights into ferredoxin-NADP(H) reductase catalysis involving the conserved glutamate in the active site, J. Mol. Biol. 397 (2010) 814–825.

[28] A. Sánchez-Azqueta, M.A. Musumeci, M. Martínez-Júlvez, E.A. Ceccarelli, M. Medina, Structural backgrounds for the formation of a catalytically competent complex with NADP(H) during hydride transfer in ferredoxin-NADP+ reductases, Biochim. Biophys. Acta 1817 (2012) 1063–1071.

[29] C.M. Bruns, P.A. Karplus, Refined crystal structure of spinach ferredoxin reductase at 1.7 Å resolution: oxidized, reduced and 2′-phospho-5′-AMP bound states, J. Mol. Biol. 247 (1995) 125–145.

[30] J. Tejero, M. Martínez-Júlvez, T. Mayoral, A. Luquita, J. Sanz-Aparicio, J.A. Hermoso, J.K. Hurley, G. Tollin, C. Gómez-Moreno, M. Medina, Involvement of the pyrophosphate and the 2′-phosphate binding regions of ferredoxin-NADP+ reductase in coenzyme specificity, J. Biol. Chem. 278 (2003) 49203–49214.

[31] M. Martínez-Júlvez, J. Hermoso, J.K. Hurley, T. Mayoral, J. Sanz-Aparicio, G. Tollin, C. Gómez-Moreno, M. Medina, Role of Arg100 and Arg264 from Anabaena PCC 7119 ferredoxin-NADP+ reductase for optimal NADP+ binding and electron transfer, Biochemistry 37 (1998) 17680–17691.

[32] V.V. Pollock, M.J. Barber, Kinetic and mechanistic properties of biotin sulfoxide reductase, Biochemistry 40 (2001) 1430–1440.

[33] P. Macheroux, UV–visible spectroscopy as a tool to study flavoproteins, Methods Mol. Biol. 131 (1999) 1–7.

[34] M. Medina, A. Luquita, J. Tejero, J. Hermoso, T. Mayoral, J. Sanz-Aparicio, K. Grever, C. Gómez-Moreno, Probing the determinants of coenzyme specificity in ferredoxin-NADP+ reductase by site-directed mutagenesis, J. Biol. Chem. 276 (2001) 11902–11912.

[35] S. Frago, I. Lans, J.A. Navarro, M. Hervás, D.E. Edmondson, M.A. De la Rosa, C. Gómez-Moreno, S.G. Mayhew, M. Medina, Dual role of FMN in flavodoxin function: electron transfer cofactor and modulation of the protein–protein interaction surface, Biochim. Biophys. Acta 1797 (2010) 262–271.

[36] V. Rodríguez-Roldán, J.M. García-Heredia, J.A. Navarro, M. Hervás, B. De la Cerda, F.P. Molina-Heredia, M.A. De la Rosa, A comparative kinetic analysis of the reactivity of plant, horse, and human respiratory cytochrome c towards cytochrome c oxidase, Biochem. Biophys. Res. Commun. 346 (2006) 1108–1113.

[37] T.E. Meyer, Z.G. Zhao, M.A. Cusanovich, G. Tollin, Transient kinetics of electron transfer from a variety of c-type cytochromes to plastocyanin, Biochemistry 32 (1993) 4552–4559.

[38] J. Tejero, J.R. Peregrina, M. Martínez-Júlvez, A. Gutiérrez, C. Gómez-Moreno, N.S. Scrutton, M. Medina, Catalytic mechanism of hydride transfer between NADP+/H

and ferredoxin-NADP$^+$ reductase from *Anabaena* PCC 7119, Arch. Biochem. Biophys. 459 (2007) 79–90.

[39] S. Daff, An appraisal of multiple NADPH binding-site models proposed for cytochrome P450 reductase, NO synthase, and related diflavin reductase systems, Biochemistry 43 (2004) 3929–3932.

[40] W. Kabsch, XDS, Acta Crystallogr. D Biol. Crystallogr. 66 (2010) 125–132.

[41] M.D. Winn, C.C. Ballard, K.D. Cowtan, E.J. Dodson, P. Emsley, P.R. Evans, R.M. Keegan, E.B. Krissinel, A.G. Leslie, A. McCoy, S.J. McNicholas, G.N. Murshudov, N.S. Pannu, E.A. Potterton, H.R. Powell, R.J. Read, A. Vagin, K.S. Wilson, Overview of the CCP4 suite and current developments, Acta Crystallogr. D Biol. Crystallogr. 67 (2011) 235–242.

[42] A. Vagin, A. Teplyakov, MOLREP: an automated program for molecular replacement, J. Appl. Crystallogr. 30 (1997) 1022–1025.

[43] P. Emsley, K. Cowtan, Coot: model-building tools for molecular graphics, Acta Crystallogr. D Biol. Crystallogr. 60 (2004) 2126–2132.

[44] A.A. Vaguine, J. Richelle, S.J. Wodak, SFCHECK: a unified set of procedures for evaluating the quality of macromolecular structure-factor data and their agreement with the atomic model, Acta Crystallogr. D Biol. Crystallogr. 55 (1999) 191–205.

[45] R.A. Laskowski, M.W. MacArthur, D.S. Moss, J.M. Thornton, PROCHECK: a program to check the stereochemical quality of protein structures, J. Appl. Crystallogr. 26 (1993) 283–291.

[46] I.W. Davis, L.W. Murray, J.S. Richardson, D.C. Richardson, MOLPROBITY: structure validation and all-atom contact analysis for nucleic acids and their complexes, Nucleic Acids Res. 32 (2004) W615–W619.

[47] J. Sancho, C. Gómez-Moreno, Interaction of ferredoxin-NADP$^+$ reductase from *Anabaena* with its substrates, Arch. Biochem. Biophys. 288 (1991) 231–238.

[48] M. Martínez-Júlvez, J. Tejero, J.R. Peregrina, I. Nogués, S. Frago, C. Gómez-Moreno, M. Medina, Towards a new interaction enzyme:coenzyme, Biophys. Chem. 115 (2005) 219–224.

[49] J.K. Hurley, M. Fillat, C. Gómez-Moreno, G. Tollin, Structure–function relationships in the ferredoxin/ferredoxin:NADP$^+$ reductase system from *Anabaena*, Biochimie 77 (1995) 539–548.

[50] M.J. Knapp, J.P. Klinman, Environmentally coupled hydrogen tunneling. Linking catalysis to dynamics, Eur. J. Biochem. 269 (2002) 3113–3121.

[51] M.J. Knapp, K. Rickert, J.P. Klinman, Temperature-dependent isotope effects in soybean lipoxygenase-1: correlating hydrogen tunneling with protein dynamics, J. Am. Chem. Soc. 124 (2002) 3865–3874.

[52] Z.D. Nagel, J.P. Klinman, A 21st century revisionist's view at a turning point in enzymology, Nat. Chem. Biol. 5 (2009) 543–550.

[53] J. Basran, R.J. Harris, M.J. Sutcliffe, N.S. Scrutton, H-tunneling in the multiple H-transfers of the catalytic cycle of morphinone reductase and in the reductive half-reaction of the homologous pentaerythritol tetranitrate reductase, J. Biol. Chem. 278 (2003) 43973–43982.

[54] A. Kohen, Kinetic Isotope Effects as Probes for Hydrogen Tunneling in Enzyme Catalysis, Isotope Effects in Chemistry and Biology, CRC Press, 2005. 743–764.

[55] J.R. Peregrina, B. Herguedas, J.A. Hermoso, M. Martínez-Júlvez, M. Medina, Protein motifs involved in coenzyme interaction and enzymatic efficiency in *Anabaena* ferredoxin-NADP$^+$ reductase, Biochemistry 48 (2009) 3109–3119.

[56] J.K. Hurley, J.L. Schmeits, C. Genzor, C. Gómez-Moreno, G. Tollin, Charge reversal mutations in a conserved acidic patch in *Anabaena* ferredoxin can attenuate or enhance electron transfer to ferredoxin:NADP$^+$ reductase by altering protein/protein orientation within the intermediate complex, Arch. Biochem. Biophys. 333 (1996) 243–250.

[57] M. Faro, C. Gomez-Moreno, M. Stankovich, M. Medina, Role of critical charged residues in reduction potential modulation of ferredoxin-NADP$^+$ reductase, Eur. J. Biochem. 269 (2002) 2656–2661.

[58] M. Martínez-Júlvez, I. Nogués, M. Faro, J.K. Hurley, T.B. Brodie, T. Mayoral, J. Sanz-Aparicio, J.A. Hermoso, M.T. Stankovich, M. Medina, G. Tollin, C. Gómez-Moreno, Role of a cluster of hydrophobic residues near the FAD cofactor in *Anabaena* PCC 7119 ferredoxin-NADP$^+$ reductase for optimal complex formation and electron transfer to ferredoxin, J. Biol. Chem. 276 (2001) 27498–27510.

[59] P.A. Karplus, M.J. Daniels, J.R. Herriott, Atomic structure of ferredoxin-NADP$^+$ reductase: prototype for a structurally novel flavoenzyme family, Science 251 (1991) 60–66.

[60] J.P. Klinman, Importance of protein dynamics during enzymatic C–H bond cleavage catalysis, Biochemistry (2013). **Q20**